Mol Biol Rep (2012) 39:3987–3993
DOI 10.1007/s11033-011-1179-2

Heat stress activates ER stress signals which suppress the heat shock response, an effect occurring preferentially in the cortex in rats

Yaohua Liu · Hiroaki Sakamoto · Masaaki Adachi · Shiguang Zhao · Wataru Ukai · Eri Hashimoto · Masato Hareyama · Tadao Ishida · Kohzoh Imai · Yasuhisa Shinomura

Received: 7 November 2010 / Accepted: 6 July 2011 / Published online: 21 July 2011

Abstract Although heat stress induces a variety of illnesses, there have been few studies designed to uncover the molecular mechanisms underlining the illnesses. We here demonstrate that heat activates ER stress, which inhibits heat shock responses (HSR) via translational block. In heat-stressed rats, ER stress responses, as represented by eIF2α phosphorylation and XBP1 splicing, occurred mainly in the cortex, where the HSR was substantially inhibited. Heat exposure also activated ER stress signals in primary cortical neurons. Since HSF1 knockdown enhanced heat-induced ER stress and subsequent cell death, HSR inhibition in turn augments ER stress, implying a vicious spiral of both stresses. Taken together, heat-induced ER stress impairs the HSR and enhances cell damage, thereby manifesting its unique effect on heat stress.

Yaohua Liu and Hiroaki Sakamoto contributed equally to this work.

Y. Liu · H. Sakamoto · M. Adachi (✉) · T. Ishida · K. Imai · Y. Shinomura
First Department of Internal Medicine, Sapporo Medical University School of Medicine, S-1, W-16, Chuo-Ku, Sapporo 060-8543, Japan
e-mail: adachi@sapmed.ac.jp

Y. Liu · S. Zhao
Department of Neurosurgery, The First Clinical College of Harbin Medical University, Nangang, Harbin 150001, People's Republic of China

W. Ukai · E. Hashimoto
Department of Neuropsychiatry, Sapporo Medical University School of Medicine, Sapporo, Japan

M. Hareyama
Department of Radiology, Sapporo Medical University School of Medicine, Sapporo, Japan

Keywords Heat shock · HSF1 · ER stress · XBP1 · eIF2α

Abbreviations

XBP1	X-box binding protein
MEF	Mouse embryonic fibroblast
ER	Endoplasmic reticulum
HSF1	Heat shock transcription factor
eIF2	Eukaryote initiation factor 2

Introduction

Molecular chaperones hold non-native polypeptides as soluble folded intermediates in a refolding competent state. Heat-shock proteins (HSPs) are molecular chaperones, and protect proteins from misfolding and aggregation caused by environmental stress or diverse diseases [1]. Heat stress rapidly activates heat shock transcription factors (HSFs) which induce HSP70 and HSP40 formation as the heat shock response (HSR). This response is crucial if denatured proteins are to refold and cells are protected from heat-induced damage, thereby placing HSF1 as the main cell survival signaling molecule against heat stress. Indeed, many reports clearly demonstrate that $HSF1^{-/-}$ MEFs are more sensitive to heat than $HSF1^{+/+}$ MEFs [2–4].

Accumulation of unfolded proteins induces ER stress, which activates many chaperone genes to refold those proteins, and is identified as the unfold protein response (UPR). ER stress activates three distinct signals: (1) attenuates translation via eIF2α phosphorylation, (2) induces ER resident molecular chaperones, Bip/GRP78 and others, (3) removes misfolded proteins via 26S proteasomes [5–7]. ER stress may follow various environmental stresses

(e.g., glucose deprivation, disturbed intracellular Ca^{2+} stores, and inhibition of protein glycosylation or degradation) [8–10], but few studies suggest a role for ER stress signals in heat-stressed cells. However, because heat induces protein unfolding and protein degradation, it seems that heat stress may induce ER stress.

We recently reported that oxidative stress impairs the HSR and enhances heat-induced cell death [11]. Interestingly, oxidative stress activates ER stress signals and inhibits refolding activity under heat stress. This suggests that the ER stress response does not protect cells from heat-mediated damage, although ER stress signals contribute to the quality control of denatured proteins and reduce ER stress burdens. These findings make it conceivable that ER stress is linked to various heat-induced illnesses. We thus addressed whether ER stress signals are activated under heat stress conditions which seems to be a crucial factor in inducing stress. We now report that heat stress clearly induces ER stress in the brain. Importantly, ER stress signals were activated preferentially in the cortex where HSP70 induction was substantially suppressed. Since this site is predominantly affected by heatstroke [12–14], ER stress may be a crucial factor affecting heat-induced cell damage.

Materials and methods

Cell culture

A human glioma cell line A172, obtained from the Japanese Cancer Research Resources Bank (Tokyo, Japan), was grown in d-MEM supplemented with 10% fetal calf serum (FCS). Viability of cells were assessed by trypan blue dye exclusion technique and cells were examined by light microscopy.

Neuronal cell cultures

As described before [15], primary cortical neurons were prepared from embryonic day 18 (E18) fetal rats (Jcl: Wistar). Cortices were dissected from embryonic brains microscopically, dissociated by trypsin (Invitrogen, Carlsbad, CA USA) treatment for 20 min at 37°C, and suspended in d-MEM with 10% FCS. After filtration, cells were washed, resuspended in a chemically defined plating medium d-MEM/B27 (Invitrogen) and plated at 0.5×10^5 cells/cm^2 on poly-L-lysine-coated tissue culture dishes. All experiments were performed on days 8–12 after culture. Serum free culture medium B27 yields nearly pure neuronal cultures (>90%), as evaluated by immunocytochemical detection of glial fibrillary acidic protein (GFAP) and microtubule-associated-protein 2 (MAP2).

Animal experiments

Wistar rats (10–15-week-old) were placed in a temperature-controlled chamber set at 45°C without anesthesia. As a pilot study, five rats were exposed to heat (45°C for 50 min) and colonic temperature was monitored using a digital thermo meter equipped with a wired thermosensor (ME-CTM303, TERUMO, Tokyo, Japan). Approximately 15 min after heat exposure, colonic temperature became about 41 ± 0.4°C. Rats were thus exposed to heat for 40 min, thereafter anesthetized with excess amount of sodium pentobarbital (100 mg/kg), killed and analyzed. Whole blood was drawn from the hepatic vein. Another five rats were used as controls. Animals used in this study were housed and treated according to the guidelines for care and use of experimental animals of the Ethics Committee of Sapporo Medical University.

Reagents and antibodies

The anti-β-actin antibody was from Sigma (St. Louis, MO). The eIF2α and anti-phospho-eIF2α antibodies were purchased from Cell Signaling Technology (Beverly, MA). The anti-14-3-3, anti-HSP70, anti-HSP40, anti-GFAP and anti-CHOP antibodies were from Santa Cruz Biotechnology Inc. (Santa Cruz, CA). The anti-Bip/GRP78 antibody was from BD Pharmingen.

Immunoblot analysis

After washing with ice-cold PBS, cells (A172 and rat primary neurons treated or untreated by heat stress) or brain tissues were lyzed by adding 200 µl of RIPA buffer (100 mM NaCl, 2 mM EDTA, 1 mM PMSF, 1% NP-40 and 50 mM Tris–HCl [pH 7.2]). Total cell lysates were collected and their protein concentrations were evaluated using a Protein Assay (BioRad, Melville, NY). The lysates (20 µg/lane) were separated by 10–15% SDS-PAGE gels and then transferred to PVDF membranes (Millipore, Bedford, MA) at 20 V for 50 min. Membranes were soaked in 5% bovine serum albumin (BSA, Sigma) overnight. The membranes were incubated with primary antibodies overnight at 4°C, and thereafter incubated with the corresponding peroxidase-linked secondary antibodies (Amersham or MBL) for 1 h at room temperature. Signals were developed by a standard enhanced chemiluminescence (ECL) method following the manufacturer's protocol (Amersham).

PCR primers

Total RNA from A172 cells, rat primary neuron cultures and brain tissues was extracted with TRIzol (BRL Life and

Technologies, MD) and cDNAs were amplified from 2 μg of total RNA using High Capacity cDNA Reverse Transcription Kit (Applied Biosystems,) with random primers. The cDNA products were analyzed on 2% agarose gel and confirmed by nucleotide sequencing. The following primer pairs were used for RT-PCR: HSP70: 5′-acaagtgtcaagagg tcatctc-3′ and 5′-ctaatctacctcctcaatggtg-3′ (human: h) or 5′-acaagtgccaggaggtcatctc-3′ and 5′-tctaatccacctcctcgatggtg-3′ (mouse and rat: m&r); HSP40: 5′-caccatgggtaaagactactaccagac-3′ and 5′-tattggaagaacctgctcaagtacggttc-3′; XBP1: 5′-ccttgtagttgagaaccagg-3′ and 5′-ggggcttggtatatatgtgg-3′ (h) or 5′-cttgtgattgagaaccaggag-3′ and 5′-ttctg ggtagacctctgggag-3′ (m&r); CHOP: 5′-atggcagctgagtca ttgcctt-3′ and 5′-cttggtgcagattcaccattc-3′ (h), 5′-tgtccagctgg gagctggaag-3′ and 5′-tgaccatgcggtcgatcagag-3′ (m&r); Bip: 5′-gagaagtttgctgaggaagacaa-3′ and 5′-ctacaactcatcttttctg1-3′; GADD34: 5′-aaaggccagaaaggtgcgcttctccg-3′ and 5′-a aaccagttggtctcagccacg-3′ (h); GAPDH: 5′-gagctgaacgg-gaagctcactggcatg-3′ and 5′-tcttactccttggaggccatgt-3′. The specificity of amplified PCR fragments was confirmed by DNA sequence analysis.

Small RNA interference

The 21-nt duplex small interfering (si) RNAs (Stealth RNAi) for human HSF1 (1: GCCUGGACAAGAAUGAG CUCAGUGA, 2: GCUCAGUGACCACUUGGAUGCUA UG) and control siRNAs (random) were purchased from Invitrogen. A172 Cells (5×10^5 cells/well in a 12-well plate) were transfected either with HSF1 siRNA or control random siRNA (siRandom) duplexes (80 nmol each) using Lipofectamine RNAiMAX (Invitrogen). After 2–4 days, cells were used for analysis for western blots and cell viability. Transfection efficiency was usually more than 50%.

Confocal microscopy

A172 cells were cultured on BSA-coated coverslips overnight, exposed to heat (42 or 45°C), incubated for the indicated hours (h) and fixed with cold methanol for 15 min. Coverslips were soaked in 5% BSA, incubated with anti-HSP70 antibody for 30 min, and thereafter incubated with Alexa Fluor 488 goat anti-rabbit IgG antibody (Molecular Probes, Eugene, OR) for 30 min. Nuclei were counterstained using propidium iodide (PI). Confocal imaging was performed using a ZEISS Pascal laser-scanning microscope.

Flowcytometric analysis

For HSP70 immunostaining, A172 cells were washed, fixed with cold 75% ethanol for 30 min at −20°C, and incubated in 0.25% Triton X-100 for 5 min at 4°C. Membrane permeabilized cells were incubated with anti-HSP70 monoclonal antibody, and subsequently incubated with AlexaFluor488-conjugated anti-mouse polyclonal antibodies, followed by analysis using a FACScan flow cytometry (Becton-Dickinson). Isotype-identical antibody or its absence was used as controls (data not shown).

Statistical analysis

Statistical significance was evaluated using Student's t test (SPSS® program, San Rafael, CA). $P < 0.05$ was considered statistically significant.

Results

We first investigated whether heat stress activates ER stress signals in human glioma A172 cells. Exposure to heat which was performed by a water bath at 40.5, 42 or 43.5°C for 40 min clearly induced eIF2α phosphorylation (Fig. 1a). The eIF2α phosphorylation was transient but clearly observed in all cells exposed to heat (Fig. 1a). Importantly, exposure to 43.5°C prolonged eIF2α phosphorylation and it neither upregulated HSP40 nor HSP70 proteins at 1–3 h after heat exposure (Fig. 1a). In addition, the stress clearly induced splicing of XBP1 mRNA, a land mark of ER stress [16] and induced GADD34, CHOP and Bip mRNA [17–19], all of which are ER stress-inducible genes (Fig. 1b). CHOP and Bip induction was comparable to that in cells treated with an ER stress inducer 0.5 mM thapsigargin (Tg; Fig. 1c). These data indicate that heat stress actually activates ER stress signals as strongly as 0.5 mM Tg [9]. Significantly, HSP40/HSP70 induction was strongly inhibited at least 3 h after heat exposure to 43.5°C, although their mRNA was clearly induced (Fig. 1a).

We further investigated the discrepant correlation between HSP40/HSP70 transcripts and their products. Short heat exposure (42 or 45°C for 20 min) similarly induced HSP40/HSP70 transcripts, and there was a distinct and persistent XBP1 splicing at 3–6 h after 45°C exposure only (Fig. 2a). Additionally, 45°C exposure clearly induced CHOP/Bip transcripts. Although both treatments transiently induced eIF2α phosphorylation, 45°C exposure induced it more persistently (Fig. 2b). Importantly, time-course analysis showed that HSP40/HSP70 protein synthesis recovered once eIF2α phosphorylation disappeared (Fig. 2b), suggesting that ER stress may inhibit HSP40/HSP70 synthesis by translational block. Flow cytometry and confocal microscopy also confirmed a different HSP70 induction pattern after 42 or 45°C exposure and the latter substantially delayed the induction (Fig. 2c, d). Interestingly, delayed HSP70 synthesis resulted in much less cytoplasmic accumulation of HSP70 at 2–6 h after 45°C exposure (Fig. 2d).

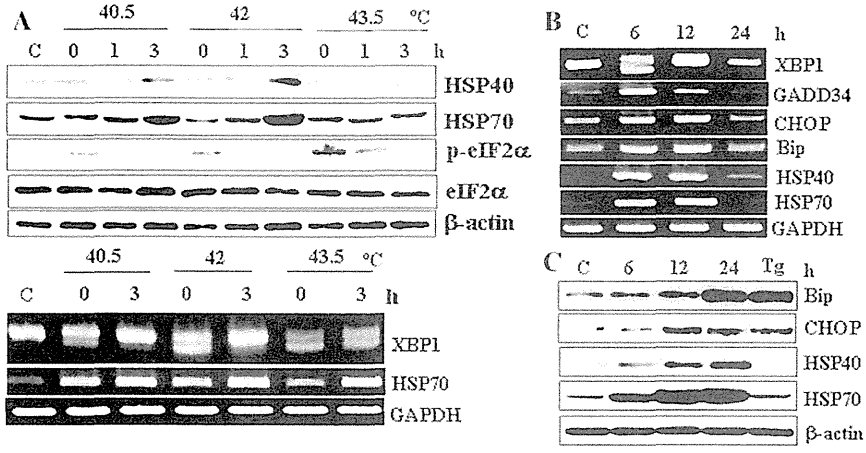

Fig. 1 HSR and ER stress signals in A172 cells. **a** HSP40/70 induction and eIF2α phosphorylation/XBP1 splicing. After exposure to heat at the indicated temperature for 40 min, the indicated proteins (*upper*) and transcripts (*lower*) were evaluated by western blots and RT-PCR, respectively, at the given hours (h). **b** XBP1 splicing and chaperone gene expression. Transcripts at the indicated hours (h) after 43.5°C exposure for 40 min were evaluated by RT-PCR. **c** Induction of HSP40/70 and ER residential chaperones. The proteins were evaluated at the indicated periods (h) after 43.5°C exposure for 40 min. As a positive control, cells were treated with 0.5 mM Tg for 12 h. All data were compared with untreated cells (C). GAPDH mRNA levels ensure that the RNAs were correctly quantified, while anti-eIF2α and anti-β-actin antibodies show equal loading of protein samples

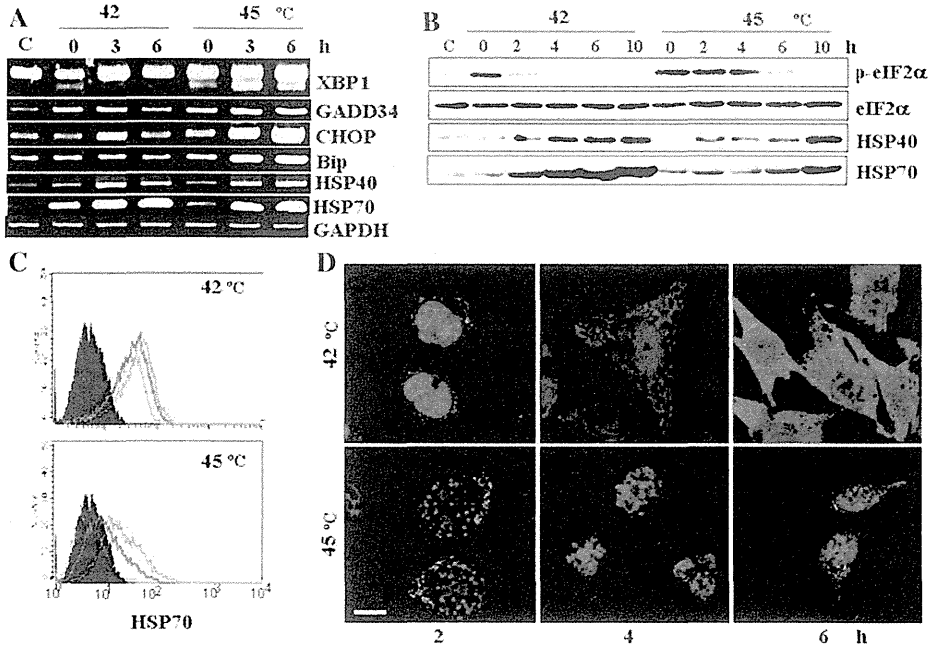

Fig. 2 ER stress and HSR inhibition in A172 cells. **a** XBP1 splicing and chaperone gene expression. Transcripts of the indicated genes at 0–3 h after 42 or 45°C exposure for 20 min were evaluated by RT-PCR. GAPDH mRNA levels ensure that the RNAs were correctly quantified. **b** HSP40/70 induction and eIF2α phosphorylation. After 42 or 45°C exposure for 20 min, the indicated proteins were evaluated at 0–10 h by western blots. **c** HSP70 induction. At 3, 6 or 9 h (*thick line*) after or before (*closed*) 42 or 45°C exposure for 20 min, HSP70 proteins were detected by flow cytometry. **d** Intracellular HSP70 localization. Cells were fixed at 2–6 h after 42 or 45°C exposure and HSP70 expression was evaluated by confocal microscopy. Nuclei were stained with PI, and control cells barely express HSP70 (data not shown)

We next investigated whether heat stress induces ER stress in rat primary neural cells. As observed in human A172 glioma cells, ER stress signals were detected after heat exposure. XBP1 splicing was distinct after exposure to more than 43.5°C and maintained for at least 8 h (Fig. 3a). Interestingly, eIF2α phosphorylation was clearly observed

in all heat-exposed cells, suggesting higher heat sensitivity than glioma cells. Time-course analysis revealed that eIF2α phosphorylation was observed 3–12 h after 45°C exposure and HSP70 began to increase after the phosphorylation diminished (Fig. 3b). In contrast, 42°C exposure did not induce prolonged eIF2α phosphorylation and clearly induced HSP70. These data indicate that heat alone induces ER stress signals similarly in both normal neuronal and malignant glioma cells. Moreover, as observed above, ER stress signals inhibit HSR probably through translational block. Conversely, HSR inhibition impairs refolding activity and leads to accumulation of unfolded proteins, thereby inducing ER stress. To explore this possibility, we inhibited HSR by transfection with siRNA which specifically binds to HSF1. HSF1 knockdown clearly suppressed HSP70 induction after 43.5°C heat exposure and augmented eIF2α phosphorylation (Fig. 3c), leading to significant increases in cell death after heat exposure (Fig. 3d). Thus, insufficient HSR indeed activates ER stress signals, implying a vicious circle of heat and ER stresses under intolerable heat stress.

We next investigated whether heat stress condition actually activates ER stress signals in the brain. Rats were placed in a dry-air chamber at 45°C for 30 min and killed immediately after heat exposure. ER stress signals were clearly activated in the whole brain, but their levels varied slightly, i.e., both XBP1 splicing and eIF2α phosphorylation were the most distinct in the cortex (Fig. 4a). Time-course study revealed that both signals quickly disappeared but were faintly detected in the cortex 1 h after heat exposure, where increased HSP70 synthesis was substantially delayed compared with the hippocampus.

In heat exposed mice, ER stress signals were similarly activated in all brain tissues, and the levels of XBP1 splicing and eIF2α phosphorylation were the highest in the cortex (Fig. 4b). Importantly, as observed in the rats, heat-mediated HSP70 induction was substantially delayed in the cortex compared with the brain stem.

Varied activation of ER stress signals under heat condition suggests that brain tissues have a different sensitivity to heat-induced ER stress. To explore the mechanism, we compared Bip expression levels in the brain tissues. Bip is localized at the ER membranes and contributes to the regulation of ER stress signals [19]. Indeed, many reports suggest that high Bip expression levels confer resistance to ER stress signals [20]. In both animals, Bip expression level was substantially lower in the cortex compared with other sites (Fig. 4c), suggesting that a lower Bip expression level may explain why cortex exhibits the highest sensitivity to ER stress in the brain.

Discussion

Considering that global warming increases the risk of exposure to a hot environment, it is crucial to understand how heat exposure induces various illnesses. Heatstroke is a life-threatening heat-induced illness, which is defined as

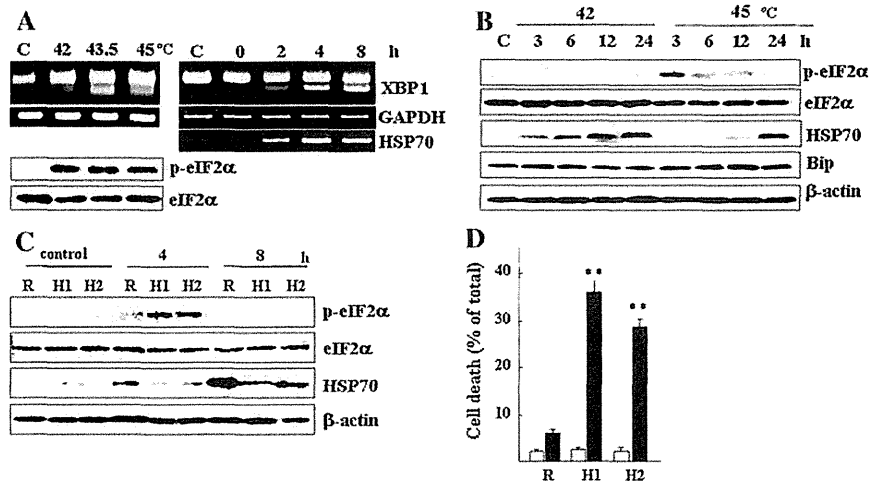

Fig. 3 ER stress and HSR inhibition in primary neurons. **a** XBP1 splicing and eIF2α phosphorylation. XBP1 splicing (*upper*) and eIF2α phosphorylation (*lower*) immediately after 42, 43.5 or 45°C exposure for 40 min. XBP1 splicing and HSP70 transcripts at 0–8 h after 45°C exposure for 20 min (*right*). GAPDH mRNA levels ensure that the RNAs were correctly quantified. **b** HSP40/70 induction. 3–24 h after 42 or 45°C exposure for 20 min, indicated proteins were evaluated. **c** Effect of HSF1 knockdown on eIF2α phosphorylation. After HSF1 knockdown (H1 or H2) or random siRNA knockdown (R), the indicated proteins were evaluated 4–8 h after 43.5°C exposure for 20 min. In **a**–**c**, anti-eIF2α and/or anti-β-actin protein antibodies show equal loading of protein samples. **d** Effect of HSF1 knockdown on cell viability. Cell death at 24 h after 43.5°C exposure for 20 min (*closed bars*) or before exposure (*open bars*). *Columns* display the mean ± SD of data from three separate experiments. $^{**}P < 0.01$ compared with random siRNA transfectants (R)

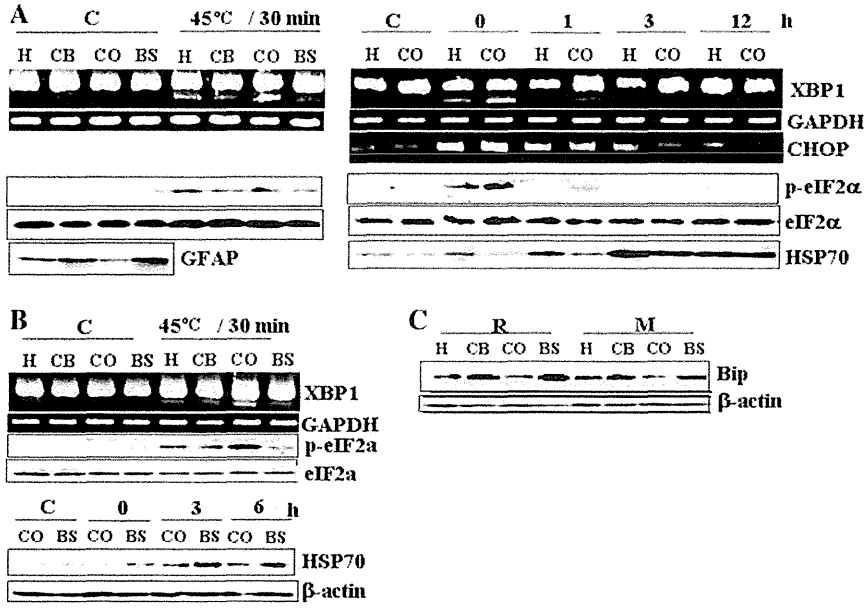

Fig. 4 Heat-induced ER stress signals in the brain. **a** ER stress signals and HSR in the rat brain. The brain samples (*H* hippocampus, *CB* cerebellum, *CO* cortex, *BS* brain stem) were harvested immediately (*left*) or at 1–3 h (*right*) after 45°C exposure for 30 min and the indicated transcripts or proteins were evaluated. **b** ER stress signals and HSR in the mouse brain. The brain samples (H, CB, CO and BS) were harvested immediately (*upper*) or at 0–3 h (*lower*) after 45°C exposure for 30 min. The indicated transcripts or proteins were evaluated. **c** Bip expression. Bip expression in the brain samples (*H* hippocampus, *CB* cerebellum, *CO* cortex, *BS* brain stem) from untreated rat (R) or mouse (M) was evaluated by western blots. GAPDH mRNA levels ensure that the RNAs were correctly quantified and anti-eIF2α or anti-β-actin protein antibody shows equal loading of protein samples

central nervous system dysfunction or failure caused by hyperpyrexia (>40°C). Pathological abnormalities in the brain have been ascribed to metabolic disorders, cerebral edema, hypoxia and ischemia [21], but it still remains unclear how heat stress causes them. We recently reported that oxidative stress inhibits HSR and augments heat-induced cell death, probably from ER stress-mediated translational block [11]. This allows us to consider that ER stress signals may have an adverse effect on biological responses to heat, although they are considered to reduce the burden of unfolded proteins and contribute to cell protection from the stress. We here demonstrate that heat induces a distinct activation of ER stress signals in the brain in vivo and reduces HSP70 induction, implying HSR inhibition. Considering that HSF1 knockdown or knockout clearly augments heat-induced cell death, ER stress-mediated HSR inhibition appears to enhance cell death. In this context, our findings enlighten a new role for ER stress signals under heat stress.

Strong heat stress activates HSP40/70 mRNA expression, but cannot increase their products, and the HSR is restored after eIF2α phosphorylation decreases. Thus, the inhibition of the HSR by ER stress signals appears to be caused by translational block due to eIF2α phosphorylation. Although heat stress itself can induce eIF2α phosphorylation via HRI [22], ER stress further enhances its phosphorylation via PERK [23]. We did not precisely investigate their activity under heat stress conditions, but both kinases should cooperatively phosphorylate eIF2α and inhibit HSR especially after exposure to strong heat stress. Obviously, further clarification as to how they function under heat stress conditions is necessary.

Our data show that the cortex has the highest sensitivity to heat-induced ER stress and the hippocampus also has a similar sensitivity. Considering that these sites are known to be primary targets of heatstroke [12–14], strong ER stress and subsequent HSR inhibition may be involved in the etiology of heatstroke. In addition, we found that these sites express Bip much less than other sites, and its expression corresponds well with ER stress sensitivity. Thus different Bip expression levels may explain why brain tissues have a different sensitivity. This idea is consistent with the previous data that Bip expression is a crucial determinant of sensitivity to ER stress [20]. In addition, our data indicates that strong HSR does not directly reflect the heat stress level, since ER stress interferes with HSR. Further studies are required to define the roles of ER stress in heatstroke and other heat-induced illnesses.

Acknowledgments Supported in part by grants from the Ministry of Education, Culture, Sports, Science, Japan (to M.A, M.H., K.I., Y.S.).

We are grateful to Dr. Peter M Olley (Sapporo Medical University School of Medicine) for editorial help.

References

1. Morimoto RI (2008) Proteotoxic stress and inducible chaperone networks in neurodegenerative disease and aging. Genes Dev 22:1427–1438
2. McMillan DR, Xiao X, Shao L, Graves K, Benjamin IJ (1998) Targeted disruption of heat shock transcription factor 1 abolishes thermotolerance and protection against heat-inducible apoptosis. J Biol Chem 273:7523–7528
3. Luft JC, Benjamin IJ, Mestril R, Dix DJ (2001) Heat shock factor 1-mediated thermotolerance prevents cell death and results in G2/M cell cycle arrest. Cell Stress Chaperones 6:326–336
4. Zhang Y, Huang L, Zhang J, Moskophidis D, Mivechi NF (2002) Targeted disruption of hsf1 leads to lack of thermotolerance and defines tissue-specific regulation for stress-inducible Hsp molecular chaperones. J Cell Biochem 86:376–393
5. Kostova Z, Wolf DH (2003) For whom the bell tolls: protein quality control of the endoplasmic reticulum and the ubiquitin-proteasome connection. EMBO J 22:2309–2317
6. Meusser B, Hirsch C, Jarosch E, Sommer T (2005) ERAD: the long road to destruction. Nat Cell Biol 7:766–772
7. Ron D, Walter P (2007) Signal integration in the endoplasmic reticulum unfolded protein response. Nat Rev Mol Cell Biol 8:519–529
8. Doerrler WT, Lehrman MA (1999) Regulation of the dolichol pathway in human fibroblasts by the endoplasmic reticulum unfolded protein response. Proc Natl Acad Sci USA 96: 13050–13055
9. Li WW, Alexandre S, Cao X, Lee AS (1993) Transactivation of the grp78 promoter by Ca^{2+} depletion. A comparative analysis with A23187 and the endoplasmic reticulum Ca(2+)-ATPase inhibitor thapsigargin. J Biol Chem 268:12003–12009
10. Wooden SK, Li LJ, Navarro D, Qadri I, Pereira L, Lee AS (1991) Transactivation of the grp78 promoter by malfolded proteins, glycosylation block, and calcium ionophore is mediated through a proximal region containing a CCAAT motif which interacts with CTF/NF-I. Mol Cell Biol 11:5612–5623
11. Adachi M, Liu Y, Fujii K, Calderwood SK, Nakai A, Imai K, Shinomura Y (2009) Oxidative stress impairs the heat stress response and delays unfolded protein recovery. PLoS One 4:e7719 (1–10)
12. Dietrich WD, Busto R, Valdes I, Loor Y (1990) Effects of normothermic versus mild hyperthermic forebrain ischemia in rats. Stroke 21:1318–1325
13. Sinigaglia-Coimbra R, Cavalheiro EA, Coimbra CG (2002) Postischemic hyperthermia induces Alzheimer-like pathology in the rat brain. Acta Neuropathol 103:444–452
14. Arumugam TV, Phillips TM, Cheng A, Morrell CH, Mattson MP, Wan R (2010) Age and energy intake interact to modify cell stress pathways and stroke outcome. Ann Neurol 67:41–52
15. Tateno M, Ukai W, Hashimoto E, Ikeda H, Saito T (2006) Implication of increased NRSF/REST binding activity in the mechanism of ethanol inhibition of neuronal differentiation. J Neural Transm 113:283–293
16. Yoshida H, Matsui T, Yamamoto A, Okada T, Mori K (2001) XBP1 mRNA is induced by ATF6 and spliced by IRE1 in response to ER stress to produce a highly active transcription factor. Cell 107:881–891
17. Mohr I, Gluzman Y (1996) A herpesvirus genetic element which affects translation in the absence of the viral GADD34 function. EMBO J 15:4759–4766
18. Oyadomari S, Mori M (2004) Roles of CHOP/GADD153 in endoplasmic reticulum stress. Cell Death Differ 11:381–389
19. Kozutsumi Y, Segal M, Normington K, Gething MJ, Sambrook J (1988) The presence of malfolded proteins in the endoplasmic reticulum signals the induction of glucose-regulated proteins. Nature 332:462–464
20. Morris JA, Dorner AJ, Edwards CA, Hendershot LM, Kaufman RJ (1997) Immunoglobulin binding protein (BiP) function is required to protect cells from endoplasmic reticulum stress but is not required for the secretion of selective proteins. J Biol Chem 272:4327–4334
21. Bouchama A, Knochel JP (2002) Heat stroke. N Engl J Med 346:1978–1988
22. Han AP, Yu C, Lu L, Fujiwara Y, Browne C, Chin G, Fleming M, Leboulch P, Orkin SH, Chen JJ (2001) Heme-regulated eIF2alpha kinase (HRI) is required for translational regulation and survival of erythroid precursors in iron deficiency. EMBO J 20:6909–6918
23. Harding HP, Zhang Y, Bertolotti A, Zeng H, Ron D (2000) Perk is essential for translational regulation and cell survival during the unfolded protein response. Mol Cell 5:897–904

Tumor Biol. (2012) 33:1307–1317
DOI 10.1007/s13277-012-0378-3

RESEARCH ARTICLE

Genome-wide analysis of DNA methylation identifies novel cancer-related genes in hepatocellular carcinoma

Masahiro Shitani · Shigeru Sasaki · Noriyuki Akutsu · Hideyasu Takagi · Hiromu Suzuki · Masanori Nojima · Hiroyuki Yamamoto · Takashi Tokino · Koichi Hirata · Kohzoh Imai · Minoru Toyota · Yasuhisa Shinomura

Received: 24 January 2012 / Accepted: 11 March 2012 / Published online: 29 March 2012

Abstract Aberrant DNA methylation has been implicated in the development of hepatocellular carcinoma (HCC). Our aim was to clarify its molecular mechanism and to identify useful biomarkers by screening for DNA methylation in HCC. Methylated CpG island amplification coupled with CpG island microarray (MCAM) analysis was carried out to screen for methylated genes in primary HCC specimens [hepatitis B virus (HBV)-positive, $n=4$; hepatitis C virus (HCV)-positive, $n=5$; HBV/HCV-negative, $n=7$]. Bisulfite pyrosequencing was used to analyze the methylation of selected genes and long interspersed nuclear element (LINE)-1 in HCC tissue ($n=57$) and noncancerous liver tissue ($n=50$) from HCC patients and in HCC cell lines ($n=10$). MCAM analysis identified 332, 342, and 259 genes that were methylated in HBV-positive, HCV-positive, and HBV/HCV-negative HCC tissues, respectively. Among these genes, methylation of *KLHL35*, *PAX5*, *PENK*, and *SPDYA* was significantly higher in HCC tissue than in noncancerous liver tissue, irrespective of the hepatitis virus status. LINE-1 hypomethylation was also prevalent in HCC and correlated positively with *KLHL35* and *SPDYA* methylation. Receiver operating characteristic curve analysis revealed that methylation of the four genes and LINE-1 strongly discriminated between HCC tissue and noncancerous liver tissue. Our data suggest that aberrant hyper- and hypomethylation may contribute to a common pathogenesis mechanism in HCC. Hypermethylation of *KLHL35*, *PAX*, *PENK*, and *SDPYA* and hypomethylation of LINE-1 could be useful biomarkers for the detection of HCC.

Keywords Hepatocellular carcinoma · DNA methylation · CpG island · LINE-1 · Biomarker

Electronic supplementary material The online version of this article (doi:10.1007/s13277-012-0378-3) contains supplementary material, which is available to authorized users.

M. Shitani · S. Sasaki (✉) · N. Akutsu · H. Takagi · H. Suzuki · H. Yamamoto · Y. Shinomura (✉)
First Department of Internal Medicine,
Sapporo Medical University,
S1, W16, Chuo-Ku,
Sapporo 060-8543, Japan
e-mail: ssasaki@sapmed.ac.jp
e-mail: shinomura@sapmed.ac.jp

H. Suzuki · M. Toyota
Department of Molecular Biology, Sapporo Medical University,
Sapporo, Japan

M. Nojima
Department of Public Health, Sapporo Medical University,
Sapporo, Japan

T. Tokino
Medical Genome Science, Research Institute for Frontier Medicine, Sapporo Medical University School of Medicine,
Sapporo, Japan

K. Hirata
First Department of Surgery, Sapporo Medical University,
Sapporo, Japan

K. Imai
Division of Novel Therapy for Cancer, The Advanced Clinical Research Center, The Institute of Medical Science,
The University of Tokyo,
Tokyo, Japan

Introduction

Hepatocellular carcinoma (HCC) is one of the most common human malignancies, worldwide [1]. Chronic infection by hepatitis B virus (HBV) and hepatitis C virus (HCV) are well-documented risk factors for the development of HCC, while chronic alcoholism and various environmental factors, including aflatoxin B1, are also believed to be important risk

factors [2, 3]. The development and progression of HCC is often a complex, multistep process entailing the evolution of normal liver through chronic hepatitis and cirrhosis to HCC, but HCC can also arise in a noncirrhotic liver. In either case, the process is influenced by multiple genetic changes, including allelic deletions, chromosomal losses and gains, DNA rearrangements, and gene mutations [4]. In addition, a growing body of evidence suggests that epigenetic changes such as DNA methylation and histone modification also play crucial roles in hepatocarcinogenesis.

Two seemingly contradictory epigenetic events coexist in cancer: global hypomethylation, which is mainly observed in repetitive sequences throughout the genome, and regional hypermethylation, which is frequently associated with CpG islands within gene promoters [5]. Hypermethylation of CpG islands is a common feature of cancer and is associated with gene silencing. Although the classical two-hit theory posits that tumor suppressor genes are inactivated by gene mutation or deletion, it is now recognized that DNA hypermethylation is a third mechanism by which inactivation of tumor suppressor genes occurs, and that it plays a significant role in tumorigenesis. In contrast to the CpG islands, repetitive DNA elements are normally heavily methylated in somatic tissues. About 45 % of the human genome is composed of repetitive sequences, including long interspersed nuclear elements (LINEs) and short interspersed nuclear element [6], and studies have shown that methylation of such repetitive elements can serve as a surrogate for the global methylcytosine content [7]. In that regard, LINE-1 hypomethylation is known to occur during the development of various human malignancies, including HCC [8, 9].

HCC is generally diagnosed at an advanced stage of tumor progression, and a large fraction of HCC cases are fatal. Thus, a better understanding of the underlying molecular mechanisms and identification of genes critical for early detection of HCC and therapeutic intervention would be highly desirable. Although a number of hyper- or hypomethylated loci have been identified in HCC [10–12], only a few studies have been conducted to unravel the genome-wide methylation status [13–15]. In the present study, we carried out genome-wide CpG island methylation analysis in a set of primary HCC specimens, with and without hepatitis virus infection. We also evaluated the hypomethylation of LINE-1 and assessed its association with aberrant CpG island hypermethylation in HCC.

Materials and methods

Tissue samples and cell lines

A total of 57 primary HCC specimens (HBV-positive, n= 21; HCV-positive, n=21; HBV/HCV-negative, n=15) were obtained through surgical resection or needle biopsy at Sapporo Medical University Hospital. Corresponding samples of noncancerous liver tissue were also obtained from 50 patients. HBV surface (HBs) antigen and anti-HCV antibody were measured serologically. An informed consent was obtained from all patients before collection of the specimens. The ten liver cancer cell lines (HT17, PLC/PRF/5, Li-7, huH-1, HuH-7, HepG2, Hep3B, HLE, HLF, and JHH-4) used have been described previously [11]. To analyze restoration of gene expression, cells were treated with 2.0 μM 5-aza-2′-deoxycytidine (5-aza-dC) (Sigma, St Louis, MO, USA) for 72 h, replacing the drug and medium every 24 h. Genomic DNA was extracted using the standard phenol–chloroform procedure. Total RNA was extracted using TRIZOL reagent (Invitrogen, Carlsbad, CA, USA) and then treated with a DNA-free kit (Ambion, Austin, TX, USA). Genomic DNA and total RNA from normal liver tissue from a healthy individual were purchased from BioChain (Hayward, CA, USA).

Methylated CpG island amplification coupled with CpG island microarray

Methylated CpG island amplification (MCA) was performed as described previously [13]. Briefly, 500 ng of genomic DNA was digested with the methylation-sensitive restriction endonuclease *Sma*I (New England Biolabs, Ipswich, MA, USA), after which it was digested with the methylation-insensitive restriction endonuclease *Xma*I. The adaptors were prepared by addition of the oligonucleotides RMCA12 (5′-CCGGGCAGAAAG-3′) and RMCA24 (5′-CCACCGCCATCCGAGCCTTTCTGC-3′). After ligation of the digested DNA to the adaptors, PCR amplification was carried out. Using a BioPrime Plus Array CGH Genomic Labeling System (Invitrogen), MCA amplicons from the HCC samples were labeled with Alexa Fluor 647, while amplicons from a normal liver sample was labeled with Alexa Fluor 555. The labeled MCA amplicons were then hybridized to a custom human CpG island microarray containing 15,134 probes covering 6,157 unique genes (G4497A; Agilent Technologies, Santa Clara, CA, USA) [16]. After washing, the array was scanned using an Agilent DNA Microarray Scanner (Agilent technologies), and the data were processed using Feature Extraction software ver. 10.7 (Agilent Technologies). The data were then analyzed using GeneSpring GX ver. 11 (Agilent Technologies).

Methylation-specific PCR

Genomic DNA (1 μg) was modified with sodium bisulfite using an EpiTect Bisulfite Kit (Qiagen, Hilden, Germany), and methylation-specific PCR (MSP) was performed as described previously [17]. Briefly, PCR was run in a 25-μl

volume containing 50 ng of bisulfite-treated DNA, 1× MSP buffer [67 mM Tris–HCl (pH 8.8), 16.6 mM $(NH4)_2SO_4$, 6.7 mM $MgCl_2$, and 10 mM 2-mercaptoethanol], 1.25 mM dNTP, 0.4 μM each primer, and 0.5 U of JumpStart REDTaq DNA Polymerase (Sigma). The PCR protocol for MSP entailed 5 min at 95°C; 35 cycles of 30 s at 95°C, 30 s at 60°C, and 30 s at 72°C; and a 7 min final extension at 72°C. Primer sequences and PCR product sizes are shown in Supplementary Table 1.

Bisulfite pyrosequencing analysis

Bisulfite pyrosequencing analysis was performed as described previously [17]. The PCR protocol entailed 5 min at 95°C; 45 cycles of 1 min at 95°C, 1 min at 60°C, and 1 min at 72°C; and a 7-min final extension at 72°C. PCR products were then bound to Streptavidin Sepharose beads HP (Amersham Biosciences, Piscataway, NJ); after which, the beads containing the immobilized PCR product were purified, washed, and denatured using a 0.2 M NaOH solution. After addition of 0.3 μM sequencing primer to the purified PCR product, pyrosequencing was carried out using a PSQ96MA system (Qiagen, Hilden, Germany) and Pyro Q-CpG software (Qiagen). Primer sequences and PCR product sizes are shown in Supplementary Table 1.

Quantitative RT-PCR

Single-stranded cDNA was prepared using SuperScript III reverse transcriptase (Invitrogen). Quantitative RT-PCR was carried out using TaqMan Gene Expression Assays (*KLHL35*, Hs00400533_m1; *PAX5*, Hs00172003_m1; *PENK*, Hs00175049_m1; *SPDYA*, Hs00736925_m1; *GAPDH*, Hs99999905_m1; Applied Biosystems, Foster City, CA, USA) and a 7500 Fast Real-Time PCR System (Applied Biosystems) according to the manufacturer's instructions. SDS1.4 software (Applied Biosystems) was used for comparative delta Ct analysis, and *GAPDH* served as an endogenous control.

Statistical analysis

To compare differences in continuous variables between groups, *t* tests or ANOVA with post hoc Tukey's tests were performed. Fisher's exact test or chi-squared test was used for analysis of categorical data. Receiver operator characteristic (ROC) curves were constructed based on the levels of methylation. Values of $P<0.05$ (two-sided) were considered statistically significant. Statistical analyses were carried out using SPSS statistics 18 (IBM Corporation, Somers, NY, USA) and GraphPad Prism ver. 5.0.2 (GraphPad Software, La Jolla, CA, USA).

Results

Genome-wide CpG island methylation analysis in HCC

To screen for CpG island hypermethylation in HCC, we carried out methylated CpG island amplification coupled with CpG island microarray (MCAM) analysis using a set of HCC tissue specimens (HBV-positive, $n=4$; HCV-positive, $n=5$; HBV/HCV-negative, $n=7$). As in an earlier study in which the same array system was used, we utilized a signal ratio (Cy5/Cy3) of >2.0 as the criterion for a methylation-positive probe [13]. The average number of methylated probe sets in the HCC specimens was 566 (range 159–846). To assess the association between hepatitis virus infection and methylation status, we categorized the HCC specimens according to their viral status. The average numbers of methylated probe sets in HBV-positive, HCV-positive, and the HBV/HCV-negative HCC specimens were 574, 598, and 539, respectively, which did not significantly differ ($P=0.840$). Interestingly, however, the numbers of methylated probe sets were more varied among HBV/HCV-negative HCCs, which is indicative of their varied pathological backgrounds (Fig. 1a).

To identify commonly methylated genes in HCC, we selected genes that were methylated in at least two tumors in each group. Among the HBV-positive HCCs, 443 probe sets (corresponding to 332 unique genes) satisfied this criterion. Among the HCV-positive HCCs, 476 probe sets (342 unique genes) satisfied the criterion, and among the HBV/HCV-negative HCCs, 348 probe sets (259 unique genes) satisfied the criterion. Collectively, 714 probes (514 unique genes) were selected as commonly methylated genes. Of those, 137, 146, and 47 probe sets were methylated in only HBV-positive, HCV-positive, or HBV/HCV-negative HCC tissues, respectively (Fig. 1b). By contrast, a large number of genes were methylated in multiple categories, and 169 probe sets were methylated in all three groups (Fig. 1b). Consistent with the above results, unsupervised hierarchical clustering analysis demonstrated that some genes were methylated irrespective of the hepatitis virus status, and that HCV-positive HCCs exhibited the largest number of methylated genes (Fig. 1c, Supplementary Fig. 1). Gene ontology analysis of the commonly methylated genes revealed that genes related to "multicellular organismal process," "developmental process," and "system development" are significantly enriched among the methylated genes (Supplementary Table 2). In addition, pathway analysis suggested that some of the methylated genes are involved in differentiation and development (Supplementary Fig. 2).

Identification of novel genes methylated in HCC

Our MCAM analysis suggested that some genes were methylated in a hepatitis virus-specific manner, but a larger

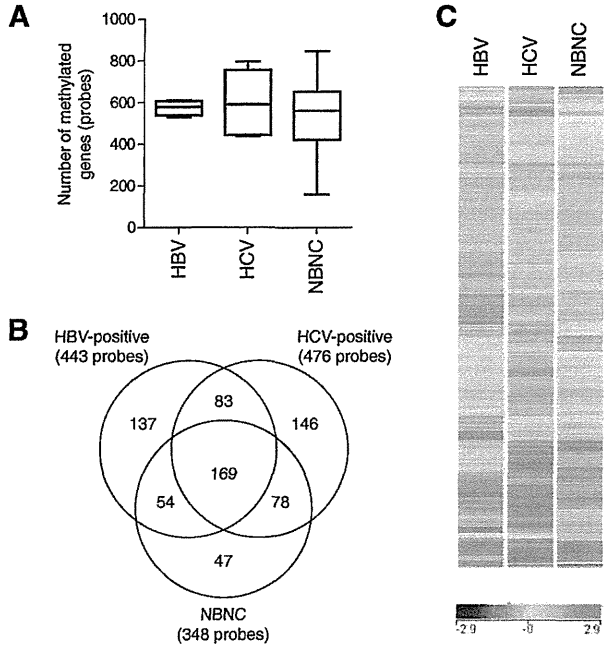

Fig. 1 Genome-wide analysis of CpG island methylation. **a** MCAM analysis was carried out using a series of HCC tissue specimens (HBV-positive, n=4; HCV-positive, n=5; HBV/HCV-negative, NBNC, n=7). MCAM data were categorized into three groups based on the hepatitis virus status, and the numbers of methylated genes in the respective categories are shown. **b** Venn diagram analysis of the methylated genes in the indicated categories. **c** Gene tree view of the MCAM analysis results. A set of 714 probes (514 unique genes) were selected as commonly methylated genes, after which, hierarchical clustering was performed. Each row represents a single probe

number were commonly methylated in HCC. Because recent studies have suggested that aberrant DNA methylation could be a useful diagnostic marker for HCC, we next aimed to identify novel genes frequently methylated in HCC. Among the genes commonly methylated irrespective of hepatitis virus status, we selected 14 (*KLHL35*, *PAX5*, *PENK*, *SPDYA*, *LTBP2*, *DLX1*, *PGBD1*, *WNT9A*, *ADRA1A*, *RHOBTB1*, *GDNF*, *WNT11*, *MLL*, and *PLEC1*) and carried out MSP to assess their methylation status in a series of HCC cell lines (Supplementary Fig. 3). We found that four (*KLHL35*, *PAX5*, *PENK*, and *SPDYA*) of the genes were frequently methylated in HCC cell lines, but showed only little or no methylation in normal liver tissue from a healthy individual (Supplementary Fig. 3). We therefore used quantitative bisulfite pyrosequencing to further analyze the methylation levels of these four genes (Supplementary Figs. 4 and 5).

To determine the extent to which these genes are aberrantly methylated in primary tumors, we analyzed a set of primary HCC specimens (HBV-positive, n=21; HCV-positive, n=21; HBV/HCV-negative, n=15) and corresponding noncancerous liver tissues from the same patients (HBV-positive, n=18; HCV-positive, n=18; HBV/HCV-negative, n=14). Bisulfite pyrosequencing analysis revealed the methylation levels of the four genes to be significantly higher in tumor tissues than in their noncancerous counterparts (*KLHL35*, 37.9 vs. 10.4 %, P<0.001; *PAX5*, 23.4 vs. 7.7 %, P<0.001; *PENK* 41.1 vs. 22.0 %, P<0.001; *SPDYA*, 49.7 vs. 19.3 %, P<0.001) (Supplementary Fig. 6). Moreover, these genes were frequently methylated in HCCs, irrespective of the hepatitis virus infection (*KLHL35*, HBV-positive, 37.5 vs. 9.9 %, P<0.001; HCV-positive, 38.3 vs. 9.0 %, P<0.001; HBV/HCV-negative, 37.7 vs. 13.0 %, P<0.001; *PAX5*, HBV-positive, 22.2 vs. 7.6 %, P=0.014; HCV-positive, 26.5 vs. 7.2 %, P<0.001; HBV/HCV-negative, 20.7 vs. 8.5 %, P=0.017; *PENK*, HBV-positive, 45.1 vs. 20.9 %, P<0.001; HCV-positive, 39.2 vs. 23.5 %, P=0.001; HBV/HCV-negative, 38.2 vs. 21.3 %, P=0.006; *SPDYA*, HBV-positive, 51.5 vs. 19.8 %, P<0.001; HCV-positive, 46.6 vs. 15.3 %, P<0.001; HBV/HCV-negative, 51.3 vs. 23.7 %, P<0.001) (Fig. 2a). The association between the methylation of each gene and the clinicopathological features are shown in Table 1. Methylation of *KLHL35* and *PAX5* was correlated with greater age, and *SPDYA* methylation was moderately correlated with higher PIVKA-II levels, but we found no other significant correlations (Table 1). We also generated an ROC curve and observed that methylation of the four genes discriminated strongly between tumor tissues and noncancerous liver tissue, suggesting that methylation of these genes could be a useful tumor marker (Fig. 2b). The most discriminating cutoffs for *KLHL35*, *PAX5*, *PENK*, and *SPDYA* were 14.8 % (sensitivity, 82.5 %; specificity, 88.0 %), 12.5 % (sensitivity, 63.2 %; specificity, 94.0 %), 28.4 % (sensitivity, 70.2 %; specificity, 96.0 %), and 30.3 % (sensitivity, 86.0 %; specificity, 94.0 %), respectively.

Analysis of *KLHL35*, *PAX5*, *PENK*, and *SPYDA* methylation and expression

We next tested whether methylation of *KLHL35*, *PAX5*, *PENK*, and *SPYDA* was associated with their silencing in HCC. Bisulfite pyrosequencing analysis revealed that the degree to which these genes were methylated varied among the HCC cell lines, but it was always much higher than in normal liver tissue from a healthy individual (Fig. 3a). Quantitative RT-PCR analysis confirmed an inverse relationship between methylation and expression of *KLHL35*

Fig. 2 Quantitative methylation analysis of the genes identified by MCAM. **a** Summary of the bisulfite pyrosequencing analysis of *KLHL35*, *PAX5*, *PENK*, and *SPDYA* in tumor tissue (*T*) and noncancerous liver tissue (*N*) from HBV-positive, HCV-positive, and HBV/HCB-negative (NBNC) HCC patients. **b** ROC curve analysis of the methylation of the indicated genes. The area under the ROC curve (*AUC*) for each site conveys its utility (in terms of sensitivity and specificity) for distinguishing between HCC tissue and corresponding noncancerous liver tissue from the same HCC patients

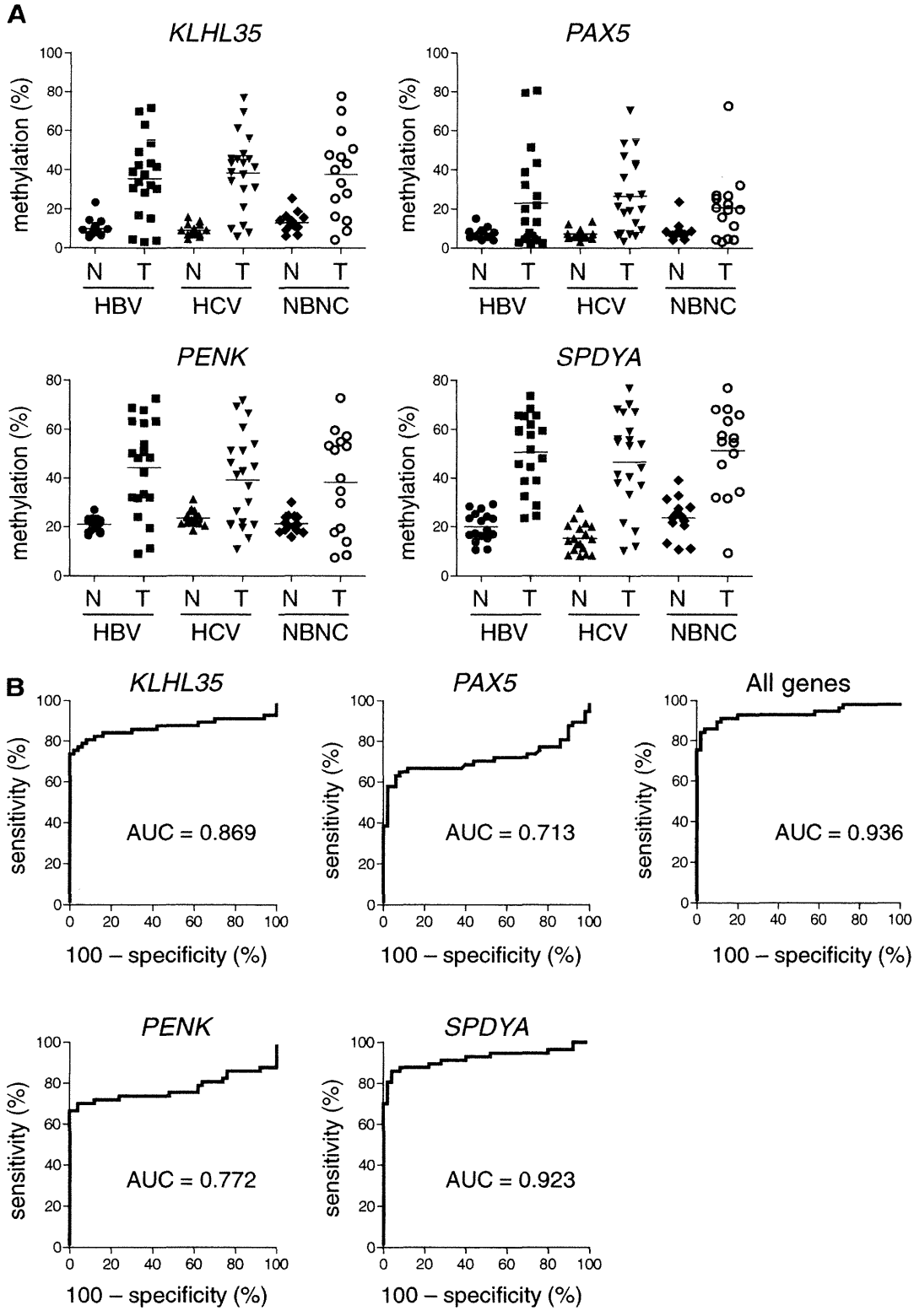

and *PAX5* in the cell lines and normal liver tissue (Fig. 3b), whereas methylation of *PENK* and *SPDYA* did not correlate significantly with their expression levels. The expression of *PENK* was undetectable in seven HCC cell lines and in

Table 1 Association between clinicopathological features and DNA methylation in HCC

	N	*KLHL35* methylation			*PAX5* methylation			*PENK* methylation			*SPDYA* methylation			LINE-1 methylation		
		Mean	SD	*P* value	Mean	SD	*P* value	Mean	SD	*P* value	Mean	SD	*P* value	Mean	SD	*P* value
Age																
≤63	24	30.3	17.7	0.003	18.3	17.1	0.026	41.7	19.3	0.583	51.2	17.9	0.945	49.4	14.8	0.571
>64	23	47.2	18.5		32.3	24.1		44.8	19.6		50.9	15.0		47.2	10.6	
Sex																
M	39	37.5	20.3		22.6	20.9		40.2	19.6		50.1	18.1		47.8	13.3	
F	18	37.2	22.0	0.953	25.2	19.9	0.652	43.1	19.6	0.602	48.7	16.7	0.771	51.5	12.0	0.318
Virus																
HBV	21	35.6	20.3		23.1	24.5		44.3	19.4		50.7	15.4		50.4	13.9	
HCV	21	38.3	19.5		26.5	19.0		39.2	18.8		46.6	19.6		50.2	12.2	
NBNC	15	36.1	22.2	0.900	20.7	17.2	0.698	38.2	21.0	0.603	51.3	18.0	0.668	44.7	12.9	0.359
Child-Pugh																
A	44	39.2	20.0		25.5	22.3		43.4	19.6		51.4	15.6		48.6	12.4	
B	3	29.7	18.2	0.426	19.9	11.8	0.672	41.0	17.1	0.842	45.3	29.5	0.536	44.6	20.6	0.609
PIVKA-II (mAU/ml)																
≤21	16	40.0	19.5		24.0	25.7		42.1	19.1		53.5	14.1		48.0	11.5	
22–66	16	35.8	11.8		23.4	14.2		44.6	14.0		42.9	15.9		52.9	10.7	
>67	15	40.1	26.9	0.795	28.3	24.8	0.802	42.8	24.9	0.933	57.1	16.6	0.039	43.8	15.1	0.136
AFP (ng/ml)																
≤7.4	16	39.3	19.3		25.8	24.1		41.4	19.0		49.4	17.0		47.4	9.2	
7.5–55.0	16	44.9	20.2		31.1	23.2		51.5	15.6		55.0	16.7		50.6	13.4	
>55.1	15	31.1	18.7	0.150	18.1	16.3	0.256	36.3	21.0	0.078	48.7	15.8	0.509	46.9	15.7	0.695
Cirrhosis																
0	27	35.3	23.4		22.2	22.2		40.0	22.1		51.8	18.2		47.7	14.7	
1	24	40.7	16.5	0.353	25.7	20.3	0.559	44.2	17.8	0.467	50.5	15.8	0.795	49.2	11.3	0.687
Vascular invasion																
0	42	38.3	18.5		24.0	21.0		43.9	19.5		52.3	15.1		48.2	12.8	
1	9	35.7	28.9	0.353	23.1	23.3	0.559	33.1	21.5	0.467	46.1	24.2	0.795	49.3	15.1	0.687
TNM stage																
1	6	29.5	15.4		15.0	9.8		50.6	12.1		43.3	20.8		58.4	11.8	
2	20	37.7	20.4		24.6	20.3		44.7	19.3		53.7	11.8		47.5	13.2	
3	13	45.4	14.3		24.4	23.4		43.0	19.3		55.5	13.8		44.8	10.6	
4	6	32.4	28.6	0.335	30.9	28.4	0.639	29.4	23.3	0.262	41.6	25.5	0.181	47.5	16.1	0.200
Multiple cancer																
0	33	38.3	22.1		26.2	23.9		43.9	20.8		51.1	18.5		48.8	14.2	
1	13	38.6	14.3	0.964	22.4	16.9	0.609	41.7	16.4	0.732	50.5	10.7	0.911	48.3	8.5	0.916

NBNC HBV/HCV-negative

normal liver tissue, irrespective of the methylation status (Fig. 3b). Conversely, although *SPDYA* was highly methylated in a majority of HCC cell lines, its expression was detectable in all cells, and most of the HCC lines exhibited greater *SPDYA* expression than did normal liver tissue (Fig. 3b). The above results suggest that *KLHL35* and *PAX5* are epigenetically silenced in HCC cells. Consistent with that idea, treating methylated cell lines with a DNA methyltransferase inhibitor, 5-aza-dC, restored the expression of *KLHL35* and *PAX5* (Fig. 3c). On the other hand, the expression of *PENK* and *SPDYA* does not appear to be affected by methylation.

Analysis of LINE-1 methylation and its association with gene hypermethylation

It was previously reported that LINE-1 is frequently hypomethylated in HCC, though most of those studies focused on HBV-positive tumors. Similarly, by using the bisulfite

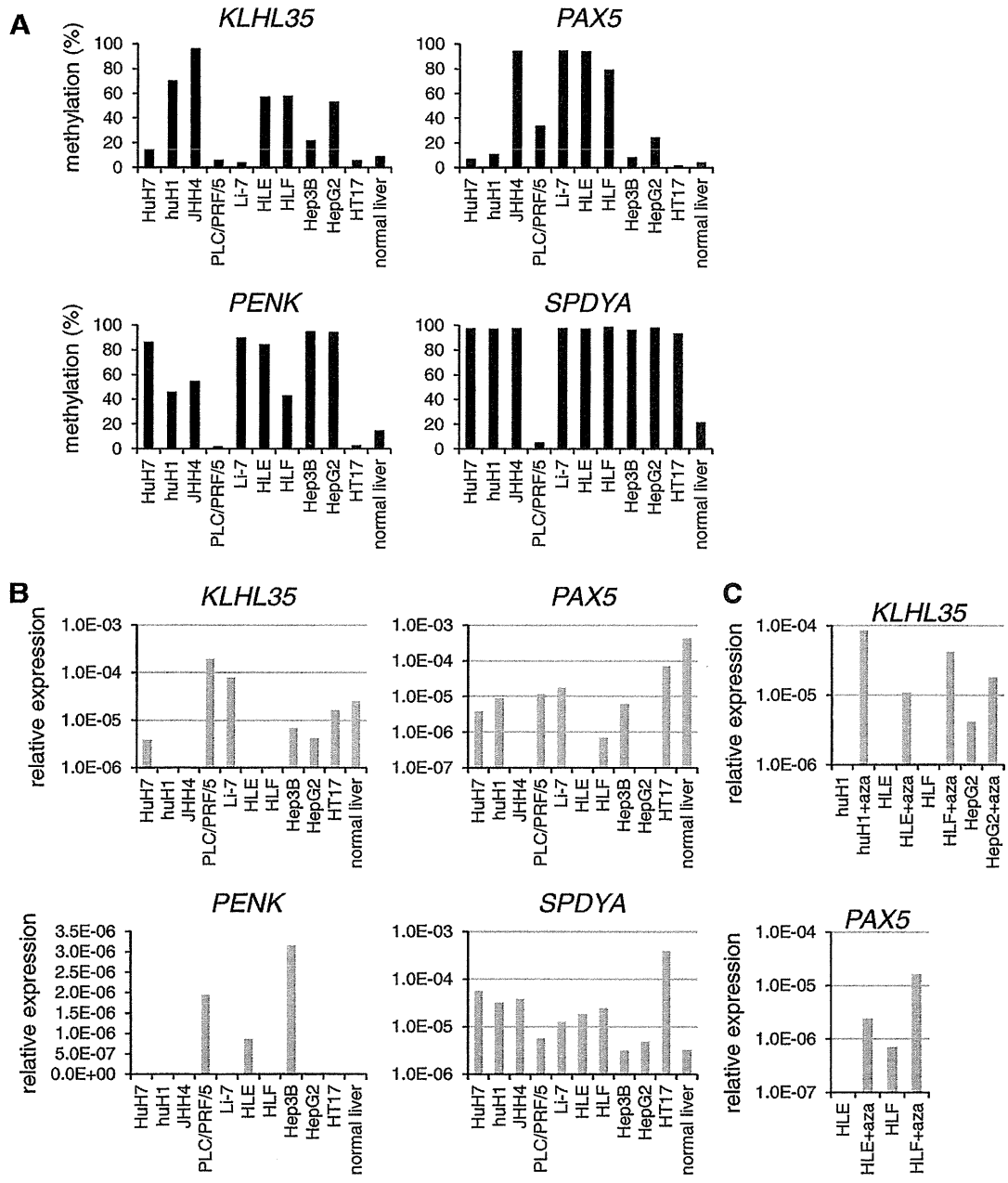

Fig. 3 Analysis of the methylation and expression of the indicated genes in HCC cell lines. **a** Bisulfite pyrosequencing of *KLHL35*, *PAX5*, *PENK*, and *SPDYA* in HCC cell lines and normal liver tissue from a healthy individual. **b** Quantitative RT-PCR of the four genes in HCC cell lines and normal liver tissue. **c** Quantitative RT-PCR of *KLHL35* and *PAX5* in HCC cell lines, with and without 5-aza-dC (*aza*) treatment

pyrosequencing, we found that levels of LINE-1 methylation were significantly lower in tumor tissues than in their noncancerous counterparts (48.5 vs. 66.8 %, $P<0.001$). LINE-1 hypomethylation was prevalent, regardless of the tumor's hepatitis virus status, but the average methylation level was lowest in the HBV/HCV-negative tumors (HBV-positive, 50.8 vs. 66.3 %, $P<0.001$; HCV-positive, 48.9 vs. 67.4 %, $P<0.001$; HBV/HCV-negative, 44.7 vs. 66.6 %, $P<0.001$; Fig. 4a). The ROC curve analysis revealed that LINE-1 methylation discriminated strongly between HCC tissue and noncancerous liver tissue (Fig. 4b), though no significant correlation was found between the levels of LINE-1 methylation and the clinicopathological characteristics of the samples (Table 1). Finally, we tested whether LINE-1 hypomethylation is linked to gene hypermethylation. We found an inverse relationship between the level of

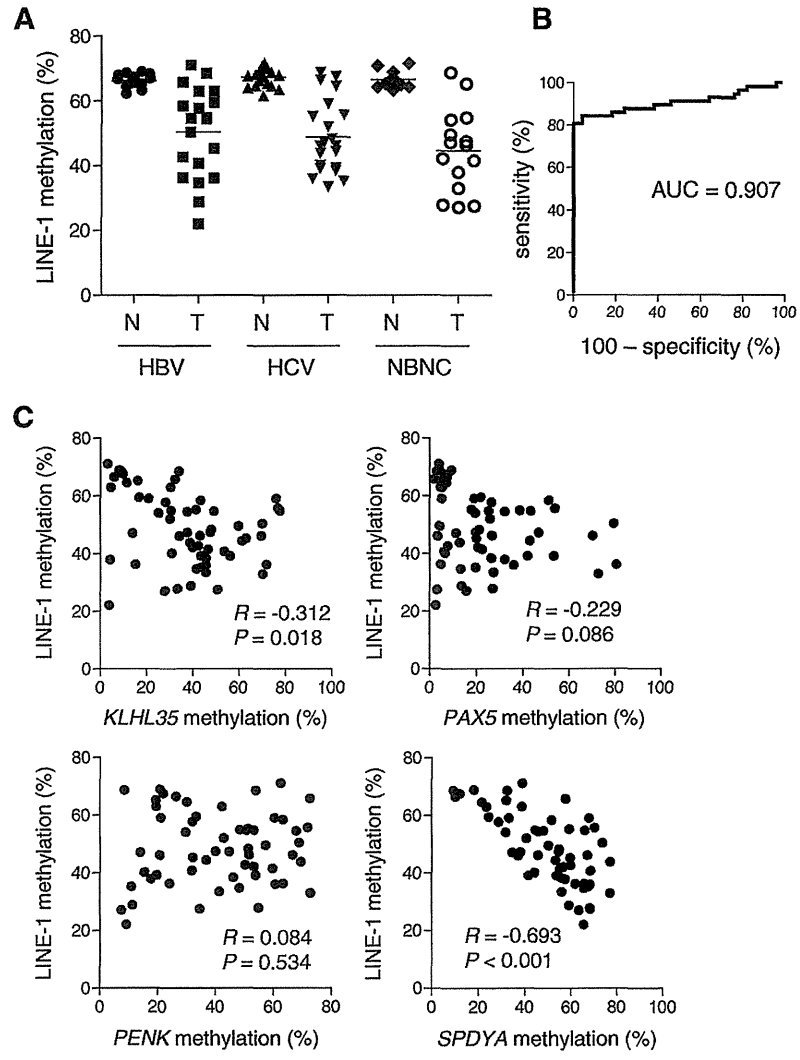

Fig. 4 Analysis of LINE-1 methylation and its association with CpG island hypermethylation in HCC. **a** Summary of bisulfite pyrosequencing analysis of LINE-1 in tumor tissue (*T*) and corresponding noncancerous liver tissue (*N*) from HBV-positive, HCV-positive, and HBV/HCB-negative (*NBNC*) HCC patients. **b** ROC curve analysis of the utility of LINE-1 methylation for distinguishing between HCC tissue and corresponding noncancerous liver tissue from the same HCC patients. **c** Correlation between the level of LINE-1 methylation and methylation of the indicated genes in HCC tissues. The Pearson correlation coefficients and *P* values are shown

LINE-1 methylation and levels of *KLHL35* and *SPDYA* methylation. On the other hand, we found no significant correlation between the LINE-1 hypomethylation and *PAX5* or *PENK* methylation (Fig. 4c).

Discussion

In the present study, we carried out high-throughput CpG island methylation profiling in a set of primary HCC tissues with and without hepatitis virus infection. MCAM analysis enabled us to evaluate the methylation status of more than 6,000 gene promoters with high specificity and sensitivity [13]. Consistent with earlier studies that showed methylation to be more abundant in the HCV-positive HCCs than in the HBV-positive or hepatitis virus-negative HCCs [15, 18], we observed the highest number of methylated genes in HCV-positive HCC tissue. However, we also noted that a large number of genes were commonly methylated among HCCs, irrespective of the hepatitis virus status, indicating that aberrant methylation of multiple genes may be involved in a common mechanism underlying hepatocarcinogenesis. Moreover, studies have also shown that aberrant methylation detected in tissues or blood samples could be a useful biomarker for early detection of HCC [19, 20]. We therefore validated the methylation status of 14 genes and identified four genes that were frequently methylated in HCC tissues but showed little or no methylation in surrounding noncancerous tissues. The high-tumor specificity suggests that methylation of these genes may not occur at precancerous stages, such as chronic hepatitis or liver cirrhosis; instead, they may be acquired during malignant transformation.

The paired box 5 (*PAX5*) gene is a member of the paired box-containing family of transcription factors, which are involved in the control of organ development and tissue differentiation [21]. PAX5 is also known to be a B cell-

specific activator protein that plays an essential role during B cell differentiation, neural development, and spermatogenesis. Methylation of the CpG island of *PAX5* was first discovered in breast cancer cells using the MCA technique [22]. Subsequently, methylation and downregulation of *PAX5* were found in lymphoid neoplasms [23]. In addition, while we are preparing the present manuscript, methylation of *PAX5* was reported in HCC and gastric cancer [24, 25]. Restoration of *PAX5* expression in HCC cells induced growth arrest and apoptosis through upregulation of various target genes, including p53, p21, and Fas ligand, suggesting that the PAX5 acts as a tumor suppressor [24].

The involvement of the kelch-like 35 (*KLHL35*) gene in cancer had not been reported until recently, when a genome-wide analysis of DNA methylation in renal cell carcinoma identified frequent hypermethylation of nine genes, including *KHLH35* [26]. Although the function of the gene product remains unknown, RNAi-induced knockdown of *KHLH35* in HEK293 cells promoted anchorage-independent growth, indicating its possible role in tumorigenesis [26].

The proenkephalin (*PENK*) gene encodes preproenkephalin, a precursor protein that is proteolytically cleaved to produce the endogenous opioid peptides met- and leu-enkephalin. Methylation of the CpG island of *PENK* was first identified in pancreatic cancer cells using the MCA technique [27]. Downregulated expression of *PENK* has also been reported in prostate cancer, suggesting its possible involvement in cancer development [28], and *PENK* methylation was recently identified in lung cancer, bladder cancer, and meningioma [29–31]. Although its functional role in cancer is not fully understood, a recent study showed that in response to cellular stress, PENK physically associates with p53 and RelA (p65) and regulates stress-induced apoptosis [32].

The *SPDYA* encodes Spy1, also known as Speedy, an atypical CDK activator known to promote cell survival, prevent apoptosis, and inhibit checkpoint activation in response to DNA damage [33]. The expression of *SPDYA* is upregulated in breast cancer [34], and its overexpression in a mouse model has been shown to accelerate mammary tumorigenesis [35]. Moreover, a recent study showed overexpression of *SYPDA* in HCC and its association with poor prognosis [36]. These results strongly suggest its involvement in oncogenesis. In the present study, we also observed that most of the HCC cell lines tested exhibited greater expression of *SPDYA* than normal liver tissue, regardless of the methylation status. Among the three transcription variants of *SPDYA* annotated in the NCBI Reference Sequence database, transcription start sites of variants 1 and 3 are located within the CpG island, while that of variant 2 are located approximately 5 kb downstream of the CpG island. Thus, the *SPDYA* transcript in HCC cells may be derived from the downstream transcription start site.

By analyzing the LINE-1 methylation levels, we and others have shown that global hypomethylation is a commonly observed feature of HCC [8, 9, 37]. Earlier studies have suggested that the association between global methylation and hepatitis status may be attributable to hepatitis B virus X protein, which can induce aberrant methylation of specific genes and global hypomethylation [38]. By contrast, we found in the present study that LINE-1 hypomethylation is prevalent among HCC tissues, regardless of the hepatitis virus infection, which suggests that global hypomethylation is involved in a common mechanism underlying hepatocarcinogenesis. It has been shown that the timing of global hypomethylation differs among tumor types. For example, hypomethylation is often observed during the early stages of colorectal and gastric carcinogenesis. By contrast, LINE-1 hypomethylation appears to be tumor-specific in HCC; it is rarely found in precancerous lesions such as chronic hepatitis or liver cirrhosis [8, 9]. A recent study showed that global hypomethylation is associated with a poorer prognosis in HCC patients [39]. In addition, the levels of serum LINE-1 hypomethylation in HCC patients reportedly correlate with serum HBs antigen status, large tumor size, and advanced tumor stage [40]. This suggests that hypomethylation may not occur at precancerous stages, and that LINE-1 methylation could be a useful biomarker with which to identify HCC and predict its clinical outcome.

The relationship between LINE-1 hypomethylation and CpG island hypermethylation in cancer is controversial. In one study, LINE-1 methylation levels were reduced in HCCs with the CpG island methylator phenotype, indicating a positive correlation between global hypomethylation and CpG island hypermethylation [9]. Another study showed that LINE-1 hypomethylation was positively correlated with hypermethylation of only a few genes (*p16*, *CACNA1G*, and *CDKN1C*), while methylation of a large number of genes showed inverse or no correlation with LINE-1 hypomethylation [12]. In the present study, we found that methylation of *KLHL35* and *SPYDA* correlates positively with LINE-1 hypomethylation, whereas levels of *PAX5* or *PENK* methylation are independent of LINE-1 methylation. These results suggest that the association between CpG island methylation and global hypomethylation may be site specific, and that hypomethylation of LINE-1 is a more generalized phenomenon than hypermethylation of CpG islands in HCC.

In summary, by screening targets of DNA methylation in HCC, we identified four frequently methylated genes. These genes are methylated in a cancer-specific manner and could be useful molecular markers for diagnosing HCC. In addition, we observed prevalent LINE-1 hypomethylation in HCC, irrespective of hepatitis virus infection. Identification of aberrant methylation in HCC may provide valuable information that not only contributes to our understanding of the pathogenesis

of the disease, but also to the development of new strategies for diagnosis and therapy.

Acknowledgments We thank Dr. Yutaka Kondo for technical advice on MCAM analysis and Masami Ashida for technical assistance. This study was supported in part by a Grant-in-Aid for Scientific Research (B) from the Japan Society for Promotion of Science (Y. Shinomura), a Grant-in-Aid for the Third-term Comprehensive 10-year Strategy for Cancer Control (M. Toyota and H. Suzuki), and a Grant-in-Aid for Cancer Research from the Ministry of Health, Labor, and Welfare, Japan (M. Toyota and H. Suzuki).

Conflicts of interest None

References

1. Parkin DM, Bray F, Ferlay J, Pisani P. Global cancer statistics, 2002. CA Cancer J Clin. 2005;55:74–108.
2. Chen CJ, Yu MW, Liaw YF. Epidemiological characteristics and risk factors of hepatocellular carcinoma. J Gastroenterol Hepatol. 1997;12:S294–308.
3. Montesano R, Hainaut P, Wild CP. Hepatocellular carcinoma: from gene to public health. J Natl Cancer Inst. 1997;89:1844–51.
4. Thorgeirsson SS, Grisham JW. Molecular pathogenesis of human hepatocellular carcinoma. Nat Genet. 2002;31:339–46.
5. Jones PA, Baylin SB. The fundamental role of epigenetic events in cancer. Nat Rev Genet. 2002;3:415–28.
6. Cordaux R, Batzer MA. The impact of retrotransposons on human genome evolution. Nat Rev Genet. 2009;10:691–703.
7. Yang AS, Estecio MR, Doshi K, Kondo Y, Tajara EH, Issa JP. A simple method for estimating global DNA methylation using bisulfite PCR of repetitive DNA elements. Nucleic Acids Res. 2004;32:e38.
8. Takai D, Yagi Y, Habib N, Sugimura T, Ushijima T. Hypomethylation of line1 retrotransposon in human hepatocellular carcinomas, but not in surrounding liver cirrhosis. Jpn J Clin Oncol. 2000;30:306–9.
9. Kim MJ, White-Cross JA, Shen L, Issa JP, Rashid A. Hypomethylation of long interspersed nuclear element-1 in hepatocellular carcinomas. Mod Pathol. 2009;22:442–9.
10. Kaneto H, Sasaki S, Yamamoto H, Itoh F, Toyota M, Suzuki H, Ozeki I, Iwata N, Ohmura T, Satoh T, Karino Y, Toyota J, Satoh M, Endo T, Omata M, Imai K. Detection of hypermethylation of the p16(ink4a) gene promoter in chronic hepatitis and cirrhosis associated with hepatitis B or C virus. Gut. 2001;48:372–7.
11. Takagi H, Sasaki S, Suzuki H, Toyota M, Maruyama R, Nojima M, Yamamoto H, Omata M, Tokino T, Imai K, Shinomura Y. Frequent epigenetic inactivation of sfrp genes in hepatocellular carcinoma. J Gastroenterol. 2008;43:378–89.
12. Lee HS, Kim BH, Cho NY, Yoo EJ, Choi M, Shin SH, Jang JJ, Suh KS, Kim YS, Kang GH. Prognostic implications of and relationship between CpG island hypermethylation and repetitive DNA hypomethylation in hepatocellular carcinoma. Clin Cancer Res. 2009;15:812–20.
13. Gao W, Kondo Y, Shen L, Shimizu Y, Sano T, Yamao K, Natsume A, Goto Y, Ito M, Murakami H, Osada H, Zhang J, Issa JP, Sekido Y. Variable DNA methylation patterns associated with progression of disease in hepatocellular carcinomas. Carcinogenesis. 2008;29:1901–10.
14. Arai E, Ushijima S, Gotoh M, Ojima H, Kosuge T, Hosoda F, Shibata T, Kondo T, Yokoi S, Imoto I, Inazawa J, Hirohashi S, Kanai Y. Genome-wide DNA methylation profiles in liver tissue at the precancerous stage and in hepatocellular carcinoma. Int J Cancer. 2009;125:2854–62.
15. Deng YB, Nagae G, Midorikawa Y, Yagi K, Tsutsumi S, Yamamoto S, Hasegawa K, Kokudo N, Aburatani H, Kaneda A. Identification of genes preferentially methylated in hepatitis C virus-related hepatocellular carcinoma. Cancer Sci. 2010;101:1501–10.
16. Goto Y, Shinjo K, Kondo Y, Shen L, Toyota M, Suzuki H, Gao W, An B, Fujii M, Murakami H, Osada H, Taniguchi T, Usami N, Kondo M, Hasegawa Y, Shimokata K, Matsuo K, Hida T, Fujimoto N, Kishimoto T, Issa JP, Sekido Y. Epigenetic profiles distinguish malignant pleural mesothelioma from lung adenocarcinoma. Cancer Res. 2009;69:9073–82.
17. Suzuki H, Yamamoto E, Nojima M, Kai M, Yamano HO, Yoshikawa K, Kimura T, Kudo T, Harada E, Sugai T, Takamaru H, Niinuma T, Maruyama R, Yamamoto H, Tokino T, Imai K, Toyota M, Shinomura Y. Methylation-associated silencing of microma-34b/c in gastric cancer and its involvement in an epigenetic field defect. Carcinogenesis. 2010;31:2066–73.
18. Nishida N, Nagasaka T, Nishimura T, Ikai I, Boland CR, Goel A. Aberrant methylation of multiple tumor suppressor genes in aging liver, chronic hepatitis, and hepatocellular carcinoma. Hepatology. 2008;47:908–18.
19. Wong IH, Zhang J, Lai PB, Lau WY, Lo YM. Quantitative analysis of tumor-derived methylated p16ink4a sequences in plasma, serum, and blood cells of hepatocellular carcinoma patients. Clin Cancer Res. 2003;9:1047–52.
20. Zhang YJ, Wu HC, Shen J, Ahsan H, Tsai WY, Yang HI, Wang LY, Chen SY, Chen CJ, Santella RM. Predicting hepatocellular carcinoma by detection of aberrant promoter methylation in serum DNA. Clin Cancer Res. 2007;13:2378–84.
21. Carotta S, Holmes ML, Pridans C, Nutt SL. Pax5 maintains cellular identity by repressing gene expression throughout B cell differentiation. Cell Cycle. 2006;5:2452–6.
22. Palmisano WA, Crume KP, Grimes MJ, Winters SA, Toyota M, Esteller M, Joste N, Baylin SB, Belinsky SA. Aberrant promoter methylation of the transcription factor genes pax5 alpha and beta in human cancers. Cancer Res. 2003;63:4620–5.
23. Lazzi S, Bellan C, Onnis A, De Falco G, Sayed S, Kostopoulos I, Onorati M, D'Amuri A, Santopietro R, Vindigni C, Fabbri A, Righi S, Pileri S, Tosi P, Leoncini L. Rare lymphoid neoplasms coexpressing B- and T-cell antigens. The role of pax-5 gene methylation in their pathogenesis. Hum Pathol. 2009;40:1252–61.
24. Liu W, Li X, Chu ES, Go MY, Xu L, Zhao G, Li L, Dai N, Si J, Tao Q, Sung JJ, Yu J. Paired box gene 5 is a novel tumor suppressor in hepatocellular carcinoma through interaction with p53 signaling pathway. Hepatology. 2011;53:843–53.
25. Li X, Cheung KF, Ma X, Tian L, Zhao J, Go MY, Shen B, Cheng AS, Ying J, Tao Q, Sung JJ, Kung HF, Yu J. Epigenetic inactivation of paired box gene 5, a novel tumor suppressor gene, through direct upregulation of p53 is associated with prognosis in gastric cancer patients. Oncogene. 2011. doi:10.1038/onc.2011.511.
26. Morris MR, Ricketts CJ, Gentle D, McRonald F, Carli N, Khalili H, Brown M, Kishida T, Yao M, Banks RE, Clarke N, Latif F, Maher ER. Genome-wide methylation analysis identifies epigenetically inactivated candidate tumour suppressor genes in renal cell carcinoma. Oncogene. 2011;30:1390–401.
27. Ueki T, Toyota M, Skinner H, Walter KM, Yeo CJ, Issa JP, Hruban RH, Goggins M. Identification and characterization of differentially methylated cpg islands in pancreatic carcinoma. Cancer Res. 2001;61:8540–6.
28. Goo YA, Goodlett DR, Pascal LE, Worthington KD, Vessella RL, True LD, Liu AY. Stromal mesenchyme cell genes of the human prostate and bladder. BMC Urol. 2005;5:17.

29. Chung JH, Lee HJ, Kim BH, Cho NY, Kang GH. DNA methylation profile during multistage progression of pulmonary adenocarcinomas. Virchows Arch. 2011;459:201–11.
30. Chung W, Bondaruk J, Jelinek J, Lotan Y, Liang S, Czerniak B, Issa JP. Detection of bladder cancer using novel DNA methylation biomarkers in urine sediments. Cancer Epidemiol Biomarkers Prev. 2011;20:1483–91.
31. Kishida Y, Natsume A, Kondo Y, Takeuchi I, An B, Okamoto Y, Shinjo K, Saito K, Ando H, Ohka F, Sekido Y, Wakabayashi T. Epigenetic subclassification of meningiomas based on genome-wide DNA methylation analyses. Carcinogenesis. 2012;33:436–41.
32. McTavish N, Copeland LA, Saville MK, Perkins ND, Spruce BA. Proenkephalin assists stress-activated apoptosis through transcriptional repression of nf-kappab- and p53-regulated gene targets. Cell Death Differ. 2007;14:1700–10.
33. Gastwirt RF, McAndrew CW, Donoghue DJ. Speedy/ringo regulation of CDKs in cell cycle, checkpoint activation and apoptosis. Cell Cycle. 2007;6:1188–93.
34. Zucchi I, Mento E, Kuznetsov VA, Scotti M, Valsecchi V, Simionati B, Vicinanza E, Valle G, Pilotti S, Reinbold R, Vezzoni P, Albertini A, Dulbecco R. Gene expression profiles of epithelial cells microscopically isolated from a breast-invasive ductal carcinoma and a nodal metastasis. Proc Natl Acad Sci U S A. 2004;101:18147–52.
35. Golipour A, Myers D, Seagroves T, Murphy D, Evan GI, Donoghue DJ, Moorehead RA, Porter LA. The spy1/ringo family represents a novel mechanism regulating mammary growth and tumorigenesis. Cancer Res. 2008;68:3591–600.
36. Ke Q, Ji J, Cheng C, Zhang Y, Lu M, Wang Y, Zhang L, Li P, Cui X, Chen L, He S, Shen A. Expression and prognostic role of spy1 as a novel cell cycle protein in hepatocellular carcinoma. Exp Mol Pathol. 2009;87:167–72.
37. Lin CH, Hsieh SY, Sheen IS, Lee WC, Chen TC, Shyu WC, Liaw YF. Genome-wide hypomethylation in hepatocellular carcinogenesis. Cancer Res. 2001;61:4238–43.
38. Park IY, Sohn BH, Yu E, Suh DJ, Chung YH, Lee JH, Surzycki SJ, Lee YI. Aberrant epigenetic modifications in hepatocarcinogenesis induced by hepatitis B virus X protein. Gastroenterology. 2007;132:1476–94.
39. Calvisi DF, Simile MM, Ladu S, Pellegrino R, De Murtas V, Pinna F, Tomasi ML, Frau M, Virdis P, De Miglio MR, Muroni MR, Pascale RM, Feo F. Altered methionine metabolism and global DNA methylation in liver cancer: relationship with genomic instability and prognosis. Int J Cancer. 2007;121:2410–20.
40. Tangkijvanich P, Hourpai N, Rattanatanyong P, Wisedopas N, Mahachai V, Mutirangura A. Serum line-1 hypomethylation as a potential prognostic marker for hepatocellular carcinoma. Clin Chim Acta. 2007;379:127–33.

釣田　義一郎
（東京大学）

Original article

doi:10.1111/j.1463-1318.2012.03108.x

Impact of family history of gastric cancer on colorectal neoplasias in young Japanese

K. Hata*, M. Shinozaki*, O. Toyoshima†, A. Toyoshima‡, S. Matsumoto†, T. Saisho† and G. Tsurita*

*Department of Surgery, the Institute of Medical Science, the University of Tokyo, Tokyo, †Department of Gastroenterology, Toyoshima Clinic, Tokyo, and ‡Department of Surgery, Japanese Red Cross Medical Center, Tokyo, Japan

Received 27 November 2011; accepted 16 February 2012; Accepted Article online 29 May 2012

Abstract

Aim The aim of this study was to elucidate risk factors for the development of colorectal neoplasia in the young population. In particular, we focused on the family history of gastric cancer.

Method Young Japanese subjects aged 30–49 years old who underwent colonoscopy for the first time from August 2007 to August 2008 were included in this study. A total of 300 unselected consecutive patients (mean age 40.5 years) were eligible for analysis, and family history of colorectal cancer and gastric cancer, sex, age, body mass index, positivity of faecal occult blood test and the presence of symptoms were evaluated. Risk factors for developing colorectal adenoma and/or carcinoma were assessed.

Results Colorectal neoplasias were detected in 83 (27.7%) cases. Two were found to have invasive carcinoma. Univariate and multivariate analyses revealed that family history of gastric cancer (OR 2.09, 95% CI 1.12–3.92, $P = 0.02$) was an independent risk factor for the development of colorectal neoplasia, as well as male sex (OR 1.89, 95% CI 1.10–3.27, $P = 0.02$), older age (OR 2.05, 95% CI 1.18–3.55, $P = 0.01$) and positive faecal occult blood test (OR 1.99, 95% CI 1.14–3.48, $P = 0.02$).

Conclusion In the young population under 50 years of age, a family history of gastric cancer is an independent risk factor for the development of colorectal neoplasia.

Keywords Colorectal neoplasia, family member, gastric cancer, Lynch syndrome, risk factor

What is new in this paper?

The most striking finding of this study is that a family history of gastric cancer proved to be an independent risk factor for the development of colorectal neoplasias in young Japanese.

Introduction

Colorectal cancer (CRC) is not only a disease of aged people but it occurs in the young as well, and CRC in the young presents as less localized and more distant disease [1]. Of CRC patients aged < 50 years, 66% presented with Stage III or IV disease [2]. Some attributed at least 50% of this to delay in the diagnosis by physicians, and the CRC could have been found earlier [3]. O'Connell *et al.* reviewed 55 articles, and 7% of all CRC patients were under 40 years of age at the time of diagnosis [4]. This is not negligible, especially from the viewpoint of life expectancy. However, from the cost–benefit viewpoint, most national guidelines recommend that CRC screening should begin at the age of 50 for the average risk population [5,6].

In Japan, the age-specific incidence of CRC was reported to be 235, 482, 862 and 1392 per 100 000 persons in the age groups 30–34, 35–39, 40–44 and 45–49, respectively [7]. The national faecal occult blood test (FOBT) screening programme has been performed for those older than 40 since 1992, but the participation rate was reported to be only 25% [8]. Therefore it is important to clarify high risk subjects for CRC and its precursor, adenoma, and to determine who in the young generation should receive colonoscopy.

Whether relatives of patients with gastric cancer have higher risk for the development of colorectal neoplasia is

Correspondence to: Keisuke Hata, MD, PhD, Department of Surgery, Institute of Medical Science, University of Tokyo, 4-6-1 Shirokanedai, Minato-ku, Tokyo 108-8639, Japan.
E-mail: khata-tky@umin.ac.jp

Preliminary data of the present study were presented at the 17th Union European Gastroenterological Week (November 2009, London).